JOURNAL OF KUFA–PHYSICS
journal.uokufa.edu.iq/index.php/jkp/index | ISSN: 2077–5830

Enhanced Thermoelectric Performance in n-type Al-doped ZnO in the Form of $(Zn_{(1-x)}Al_x)O$

***Nisreen Gh.Abdul-Nabi** **Arej Kadhim**

Dep. of physics, college of education for pure science, university of Babylon, Iraq.

*Corresponding Author E-mail: nisreen.shamlan.sci@uobasrah.edu.iq

ARTICLE INF.

Article history:
Received: 22 MAY., 2023
Revised:02 DEC., 2023
Accepted: 04 DEC., 2023
Available Online: 20 DEC., 2023

Keywords:

Thermoelectric properties
Thermoelectric materials
ZnO
Al
Solid state reaction

ABSTRACT

Compositions of $(Zn_{(1-x)}Al_x)O$ were synthesized via the Solid-state reaction (SSR) technique at $1000°C$, with x ranging from $0.005\ to\ 0.03$. After the preparation of the sample, the structure and thermoelectric properties were examined by XRD, SEM, and EDX and the home-built equipment, respectively. All the samples are observed to be polycrystalline and hexagonal structures. The composition with $(x = 0.015)$, i.e. $(ZnO_{(0.985)}Al_{0.015})$, exhibited the highest electrical conductivity values$\sim 55000\ S/m$ at $580K$. As well as for the Seebeck coefficient, it was discovered that the composition $(ZnO_{(0.98)}Al_{0.02})$ had the highest values $\sim -400\ \mu v/K$ at $680\ K$. The power factor (PF) for the composition with the formula $(ZnO_{(0.98)}Al_{0.02})$ was found to have the most outstanding possible value of $\sim 1300\ \mu w/mK^2$ at $580\ K$.

DOI: https://doi.org/10.31257/2018/JKP/2023/v15.i02.12137

تعزيز الاداء الكهروحراري لاوكسيد الخارصين (ZnO) المطعم بالالمنيوم (Al) من النوع n بالصيغة الرياضية $(Zn_{(1-x)}Al_x)O$

نسرين غازي عبد النبي **أريج كاظم عباس**

جامعة البصرة ،كلية العلوم ، قسم الفيزياء ، البصرة ، العراق

الـــخُـــلاصـــة

التركيبات بالصيغة $(Zn_{(1-x)}Al_x)O$ تم تصنيعه باستخدام طريقة تفاعل الحالة الصلبة (SSR) عند درجة حرارة 1000 درجة سيليزيه ، حيث تتدرج قيم x من 0.005 الى 0.03. تم فحص البنية الهيكلية باستخدام قياسات XRD ، SEM، و EDX وقد لوحظ أن جميع العينات عبارة عن هياكل متعددة البلورات وسداسية. كما تم قياس الخواص الكهروحرارية باستخدام ادوات مصنعة مختبريا .أظهرت التركيبة ذات(x = 0.015) ، أي $(ZnO_{0.985}Al_{0.015})$ ، أعلى قيم التوصيل الكهربائي $\sim 55000\ S/m$ عند $580K$. وكذلك بالنسبة لمعامل سيبيك، وجد أن التركيبة $(ZnO_{0.98}Al_{0.02})$ لديها أعلى القيم $\sim -400\ \mu v/K$ عند $680\ K$ اما عامل القدرة (PF) تم العثور على التركيبة ذات

الكلمات المفتاحية:

الخواص الكهروحرارية :
المواد الكهروحرارية
أوكسيد الخارصين
الالمنيوم
تفاعل الحالة الصلبة

الصيغة $(ZnO_{0.98}Al_{0.02})$لتكون لها القيمة الممكنة الأكثر تميزًا وهي / 1300 µw~
(mK^2)عند 580 K.

1. Introduction

One of the most actively pursued research areas at the present days is the development of different forms of energy production technologies, particularly thermoelectric (TE) power generation [1]. A tremendous quantity of waste heat may be transformed into usable energy, for example, the heat from automobiles, various technological processes, and anthropogenic impacts help to boost manufacturing efficiency and enhance living circumstances[2].

TE power production depends on the Seebeck effect, which mainly includes the production of electromotive force (voltage) between both the opposite edges of a metal rod underneath a particular difference in temperature. As soon as connecting an electric circuit to this metal rod, an electric current passes through the circuit to produce electric power. In this way, heat may be transformed into electricity[3-5].

The materials required for TE applications must be nontoxic, produced from naturally plentiful elements, and have excellent chemical and thermal stability [6]. These stand in as the primary benefits of oxide-based thermoelectric materials above conventional TE materials [7]. One of them is zinc oxide (ZnO), ZnO belongs to group II-VI of semiconductors, which has always been a fascinating division of semiconductors. The crystal structure of II-VI compounds often takes the form of a cubic or hexagonal structure. The majority of these compounds may be found in a variety of band gaps and lattice constants. (ZnO) has a large band gap ($3.4\ eV$) and a self-activated hexagonal wurtzite structure [8-10]. Un-doped ZnO displays n-type conductivity because of inherent flaws in the ZnO lattice [11, 12]. ZnO is an excellent thermal conductor with a high thermal capacity in terms of its thermal characteristics The TE characteristics and performance of ZnO may be altered by doping or co-doping by creating additional electrons, for example, by swapping Zn^{2+} ions with group III ions such as aluminum Al [13]. Al has utilized the dopant element because it is a plentiful, low-cost substance with a modest ionic radius [14-16].

In this article, we show how to use the solid-state reaction method at $1000°C$ to Synthesis $(Zn_{(1-x)}Al_x)$O ceramics with x ranging from $0.005\ to\ 0.03$. Calculations were made on the electrical conductivity σ, Seebeck coefficient S, and power factors PF of thermoelectric materials at temperatures ranging from 300 to $573K$.

2. Experimental technique

By using the traditional solid-state reaction method, we used high-purity ZnO (99.5% pure powder) and Al (99.5% pure powder) as raw materials for the synthesis of $(Zn_{(1-x)}Al_x)$O pellets, where x ranges from $0.005\ to\ 0.03$. These powders were mixed by adding a small amount of $(CH_3)_2Co$ to start the mixing process, and inserting an agate and pestle for five hours To obtain a homogeneous compound with a nanostructure, After that, the resulting powders were compressed for 10 minutes at a pressure of 10 tons. Then the result was sintered in a Muffle Furnace at $1273K$ for three hours.

XRD measurements were used to investigate the phase composition and crystal structure of Al-doped ZnO samples. $Cu-K$ 1.54060 Å and a generator of $30mA$ and $40kV$ were utilized in the XRD equipment. The XRD scanning ranged from 10° to 80°. Scanning electron microscopy (SEM) and energy-dispersive X-ray spectroscopy (EDX) JSM-6460LV module were used to characterize the

surface morphology and the stoichiometric ratio of each element, respectively, from chosen materials.

The van der Pauw technique was used to calculate the Hall coefficient and carrier concentration of the samples with an applied magnetic field of $1\ T$.

The Seebeck coefficient S, electrical conductivity σ, and thermoelectric power factor PF were measured at $300-573\ K$. The Van der Pauw four-probe method was used to measure electrical conductivity as a function of temperature at a pressure of 10^{-3} mbar. To compute the Seebeck coefficient the pellet had one end connected to a hot side (heater) and the other end connected to a cold side. The hot and cold sides' temperatures were gradually raised from room temperature to $573K$ at regular intervals of $5°C$, and they were measured using a thermocouple. (type-K E©Sun ECS820C).

3. Results and Discussion

XRD patterns were used to examine the crystal structures of the samples. Figure (1) displays all samples characterized by hexagonal structure and can be seen to agree well with the $JCPDS\ 36-1451$. The dominant peak represents the plane (101) at an angle of $36.2°$ with a small peak of Al at the plane (200) agreed well with the $JCPDS\ 04-0787$, this might be a result of the low Al concentration as shown in Figure (1), which is fully absorbed into the ZnO crystal and impossible to detect. It is dispersed atomically throughout the ZnO crystal or limited to the grains of ZnO nanocrystals [17]. The lattice constant parameters (a and c) are listed versus the Al content as shown in Table 1 and Figure 2 Increasing the lattice parameters that attributed to substitution of Al atomic radius ~ 0.143Å for the larger Zn atomic radius ~ 1.38Å. These findings indicated the solid-state reaction method was a sensible technique for Al atoms to enter the crystal lattice of $(ZnO)_{1-x}Al_x$ successfully [18] .The Scherrer equation can be used to calculate the average grain size [19], where.

$D=\frac{0.9\,\lambda}{\beta\ Cos\theta}$, D is the average particle size, β is the full width of half maximum of the peaks in radian, λ is the X-ray wavelength, and θ is Bragg's angle [20].

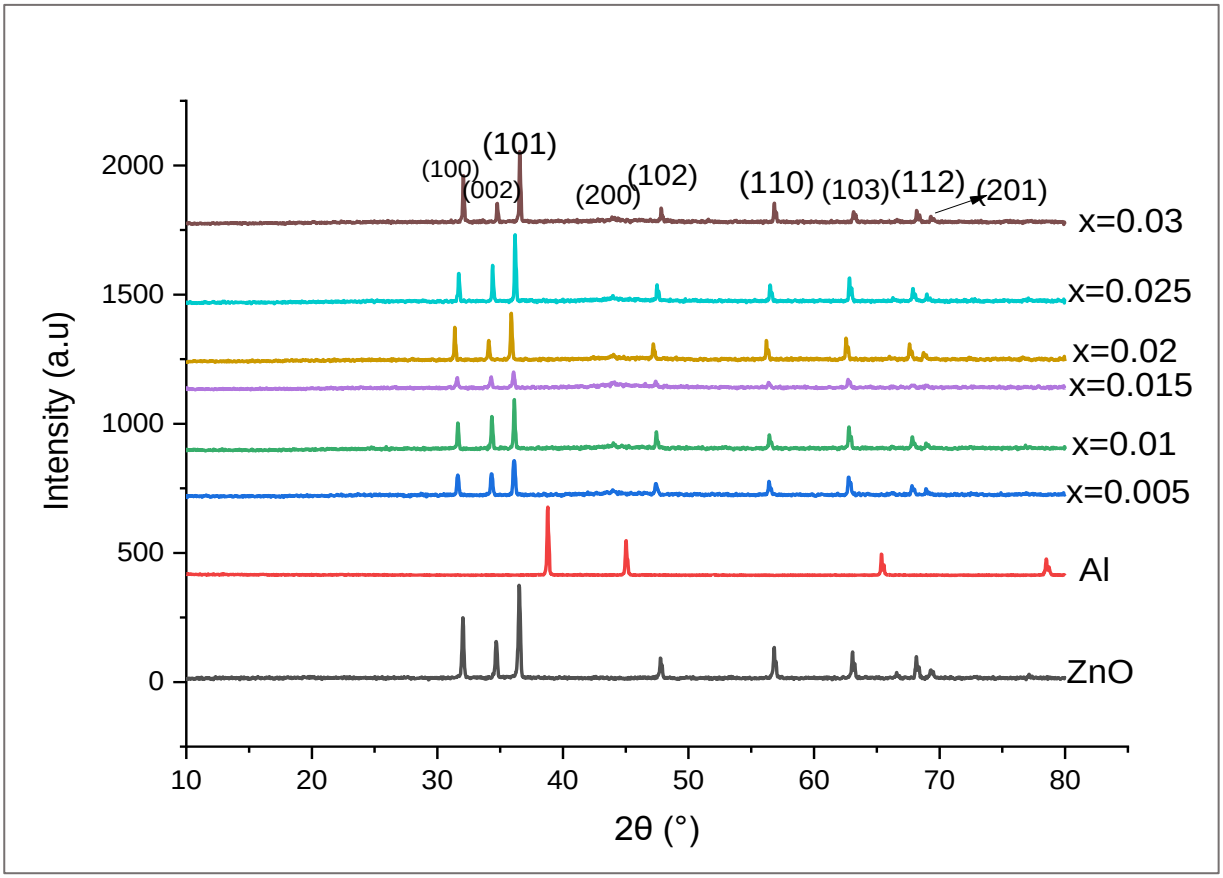

Figure 1: The XRD diffraction spectra of the pure ZnO, pure Al and $(Zn_{(1-x)}Al_x)$O pellets, with $x = 0.005, 0.01, 0.015, 0.02, 0.025, and\ 0.03$.

Table 1:Lattice parameters and particle size for the $(Zn_{(1-x)}Al_x)$O pellets, with $x = 0.005, 0.01, 0.015, 0.02, 0.025, and\ 0.03$

x	$(ZnO)_{1-x}Al_x$	2θ°	FWHM	d(Å)	a (Å) $= b$(Å)	c (Å)	D(nm)
0.005	$(ZnO)_{0.995}Al_{0.005}$	36.39	0.236	2.487	3.267	5.335	60.763
0.01	$(ZnO)_{0.99}Al_{0.01}$	36.12	0.098	2.486	3.198	5.222	70.455
0.015	$(ZnO)_{0.985}Al_{0.015}$	36.06	0.118	2.458	3.213	5.248	70.889
0.02	$(ZnO)_{0.98}Al_{0.02}$	35.88	0.098	2.502	3.219	5.257	84.923
0.025	$(ZnO)_{0.975}Al_{0.025}$	36.18	0.098	2.482	3.235	5.283	84.995
0.03	$(ZnO)_{0.97}Al_{0.03}$	36.57	0.157	2.937	3.257	5.320	85.088

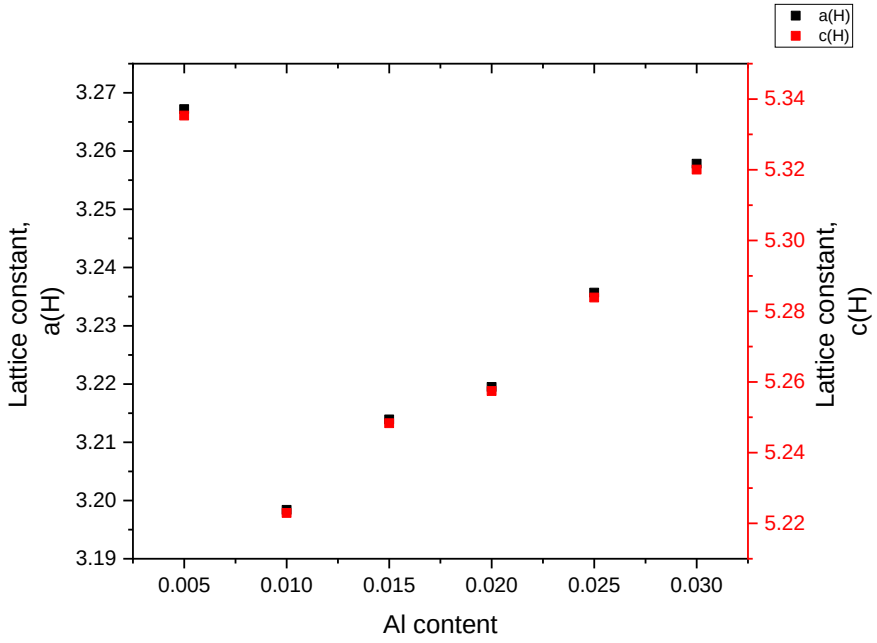

Figure 2: Lattice parameters a (Å) and c(Å) as a function of Al content.

Scanning electron microscopy (SEM) images of the $(Zn_{(1-x)}Al_x)$O pellets are shown in Figure 3a–d. X-ray diffraction and scanning electron microscopy were seen to be in good agreement. Figure 2 demonstrates having a flat surface, The growth of the grains is still by pinning the grain boundaries and, as a result, reducing their mobility [21]. Figure 4 and Table 2, show the EDX spectra of selected area on the $(ZnO)_{1-x}Al_x$ surface illustrate the distribution of the individual , Al, and O elements inside the nanoparticles, demonstrating the homogeneous entrance of the Al atoms into ZnO lattice structures.

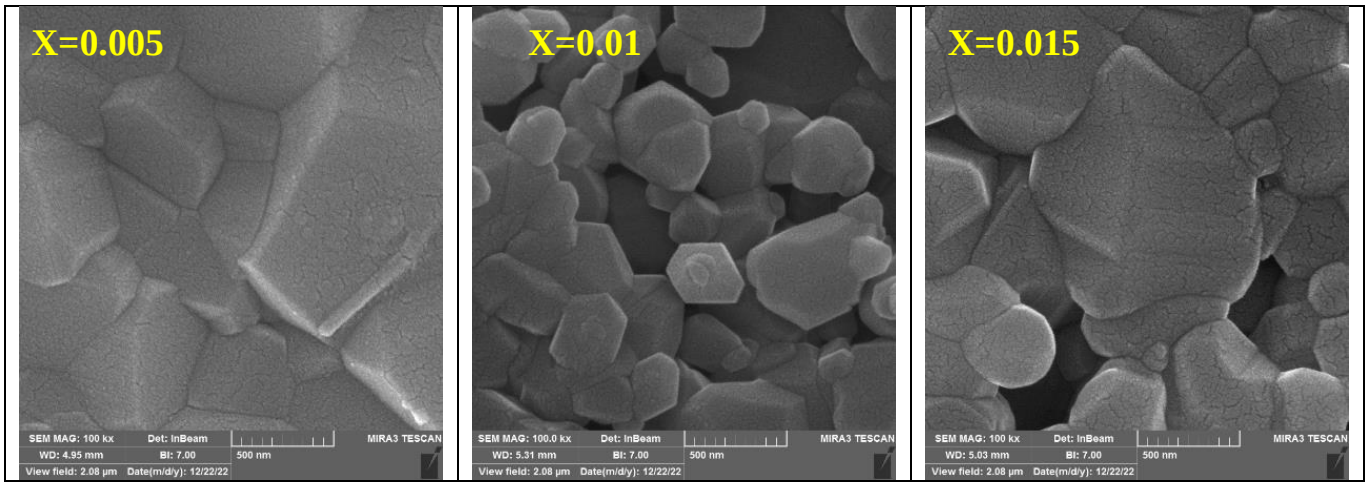

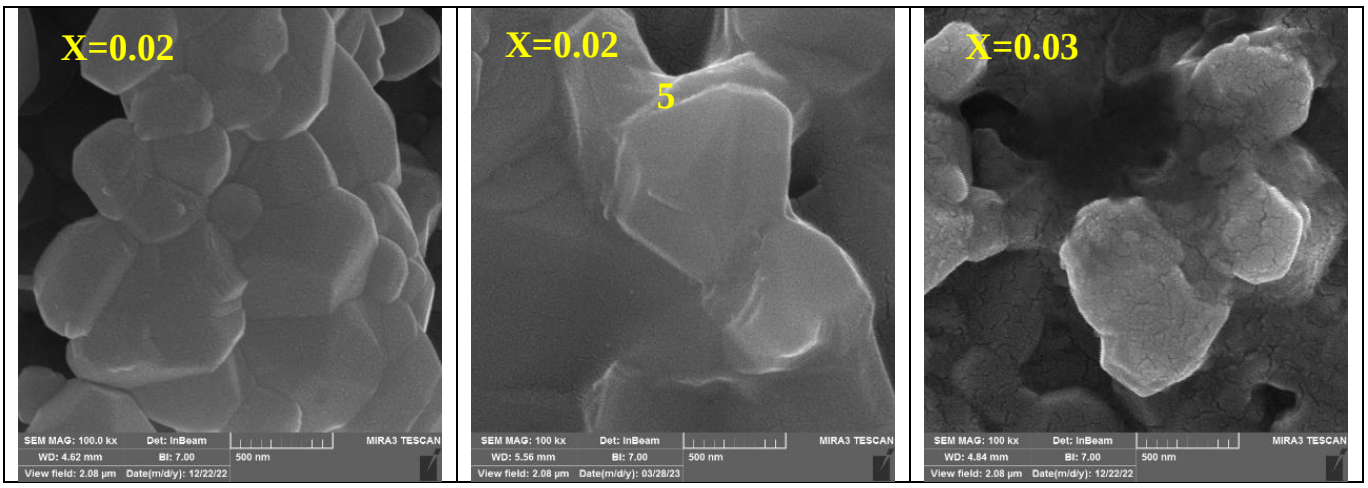

Figure3: SEM images of the $(Zn_{(1-x)}Al_x)O$ sample, with x = 0.005, 0.01, 0.015,0.02,0.025, and 0.03.

Figure 4 shows the equivalent EDX elemental mapping patterns of $Zn, O,$ and Al. These graphs demonstrate the distribution of the individual , Al, and O elements inside the nanoparticles, demonstrating the homogeneous dispersion of the Al dopant.

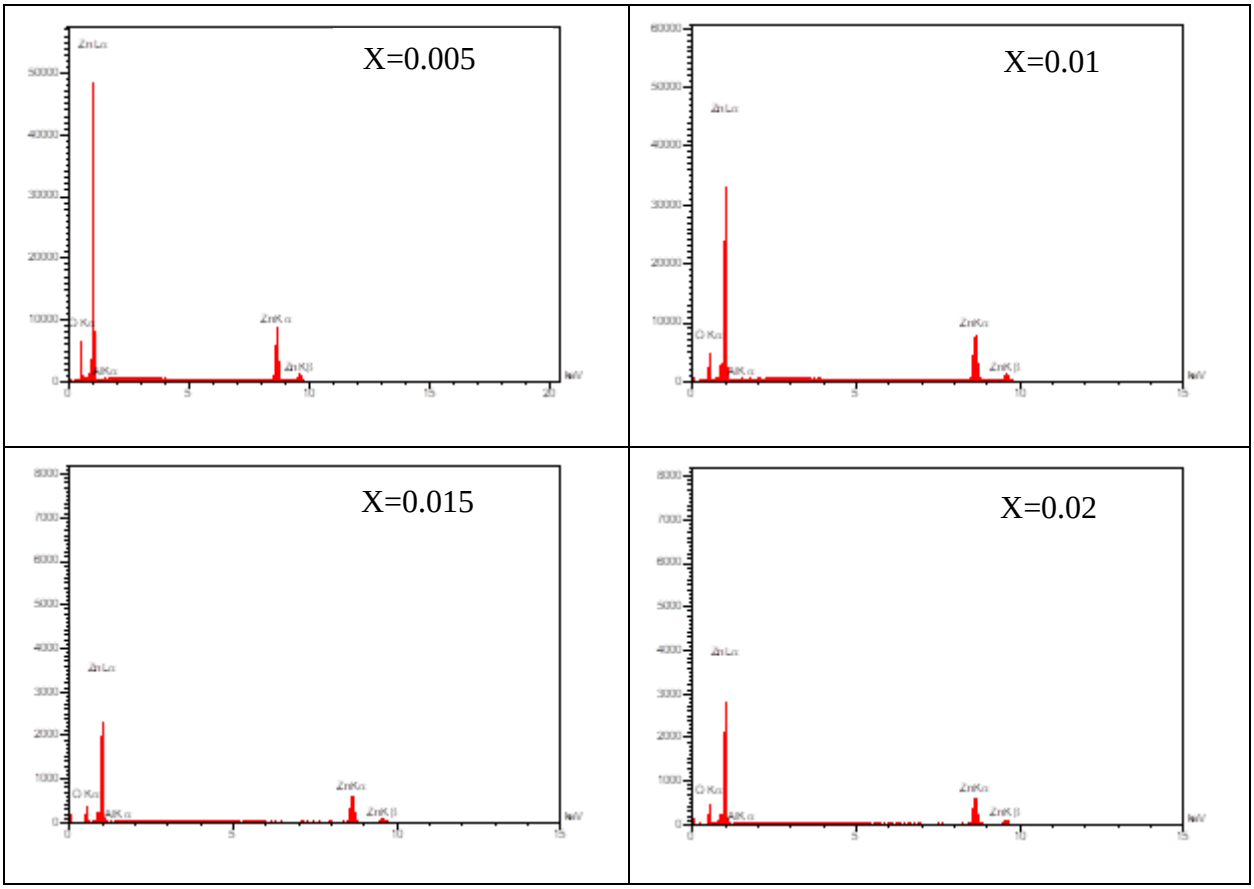

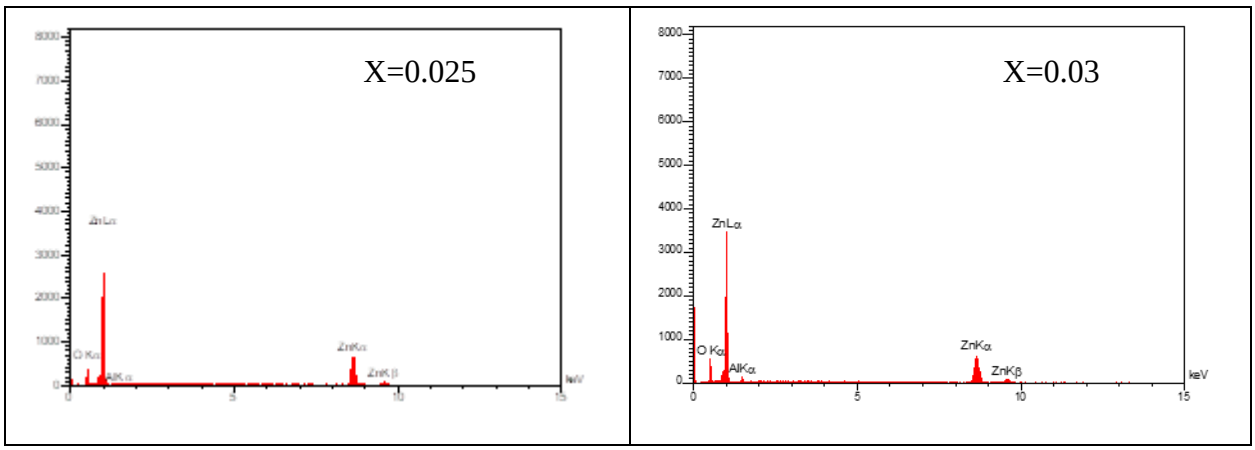

Figure 4:EDX images of the $(Zn_{(1-x)}Al_x)$O. sample with $x = 0.005, 0.01, 0.015, 0.02, 0.025, and\ 0.03$.

Table 2: EDX elemental composition results $(ZnO)_{1-x}Al_x$ pellet.

Sample $(Zn_{(1-x)}Al_x)O$	Element	Weight%	Atomic%
$ZnO_{0.995}Al_{0.005}$ $x = 0.005$	O	34.69	66.81
	Al	3.57	4.08
	Zn	61.74	29.10
$ZnO_{0.99}Al_{0.01}$ $x = 0.01$	O	30.11	61.97
	Al	3.96	4.83
	Zn	65.93	33.20
$ZnO_{0.985}Al_{0.015}$ $x = 0.015$	O	30.12	61.91
	Al	4.09	4.98
	Zn	65.80	33.10
$ZnO_{0.98}Al_{0.02}$ $x = 0.02$	O	33.99	65.73
	Al	4.51	5.17
	Zn	61.50	29.10
$ZnO_{0.975}Al_{0.025}$ $x = 0.025$	O	26.90	57.70
	Al	5.26	6.69
	Zn	67.84	35.61
$ZnO_{0.97}Al_{0.03}$ $x = 0.03$	O	30.33	58.90
	Al	11.83	13.62
	Zn	57.84	27.48

Figure 5 presents the temperature dependence of the electrical conductivity σ. The Al atom has three valence electrons, whereas, the Zn atom has only two, replacing $Zn^{2+}$with Al^{3+}introduces one more electron into the lattice. The addition of Al in the lattice results in the addition of donor levels to the band structure. This additional electron is excited from donor energy levels into the conduction band, which raises the sample's electrical conductivity[22]. All the investigated samples showed a semiconducting behavior over the whole measured temperature range[22, 23], i.e. the electrical conductivity increases with increasing temperature [24]. The maximum electrical conductivity is $55000\ s/m$ for $ZnO_{0.985}Al_{0.015}$ at $573\ K$.

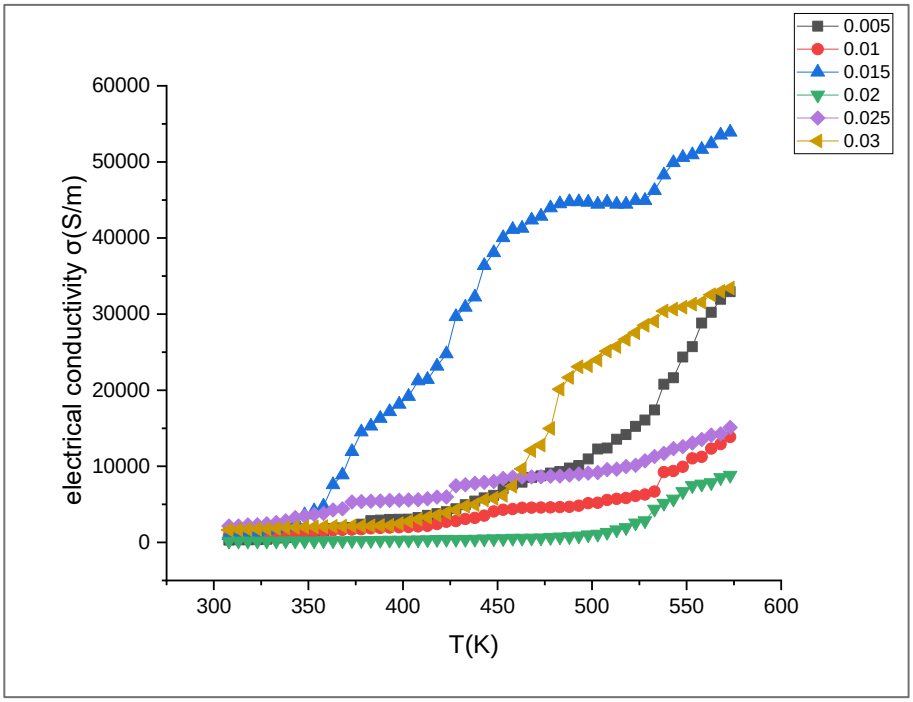

Figure 5: The electrical conductivity of the $(Zn_{(1-x)}Al_x)$O pellets, with $x = 0.005, 0.01, 0.015, 0.02, 0.025, and\ 0.03$.

Figure 6 presents the Seebeck coefficient S of the sintered samples. The S phenomenon happens when there is a significant temperature differential between the hotter and colder ends of a semiconductor. The fact that the Seebeck coefficient values are always negative over the whole temperature range and for all of the samples which demonstrates that the semiconductor in question is of the n-type kind, which has electrons as the predominant form of charge carrier. [15, 25, 26]. Figure 5 makes it abundantly evident that there is a correlation between a rise in temperature and an increase in the absolute values of S [18].The S has a correlation that is inversely proportional to the number of carriers. (Eq. 1)[27, 28]. The electrons at the Fermi level will move into the conduction band as the temperature rises. The highest S was studied for the composition with $x = 0.02 \sim -450\ \mu V/K$ at 680K. The S can be expressed as:

$$S = \frac{k}{e}\left[\left(r + \frac{5}{2}\right) + \ln\left(\frac{2(2\pi m^* kT)^{3/2}}{h^3 n}\right)\right] \quad (1)$$

Where (k, e, r, m^*, h, n) is Boltzmann's constant, the electron charge, scattering factor, effective mass, Planck constant, and carrier concentration [29].

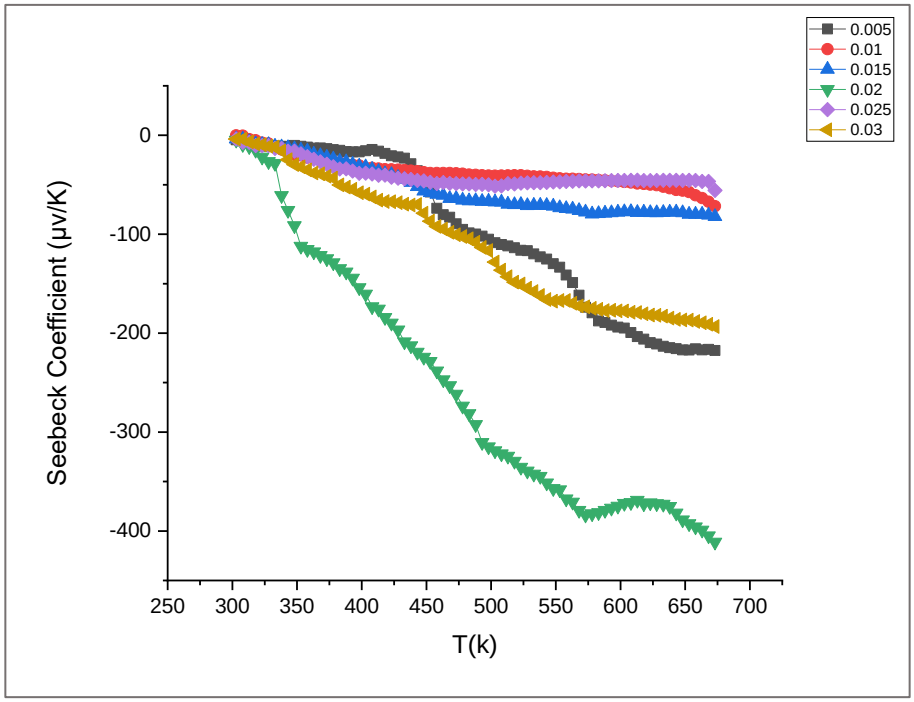

Figure 6: The Seebeck coefficient of the $(Zn_{(1-x)}Al_x)$O pellets, with $x = 0.005, 0.01, 0.015, 0.02, 0.025, and\ 0.03$.

The van der Pauw method was used to find the value of (n) in a magnetic field with an intensity of 1 tesla. In order to determine the carrier concentration, the following formula was used[30]:

$$n = \frac{IB}{ed|V_H|} \qquad (2)$$

The symbols "B" "I" "V_H" and "d" respectively, are used to designate the magnetic field, direct current, Hall voltage, pellet thickness, and electronic charge, respectively. Additionally, the pellet carries an electrostatic charge. The Hall coefficient $R_H$may be expressed using the formula provided below [30, 31].

$$R_H = \frac{1}{ne} \qquad (3)$$

The link that exists between n and R_H is illustrated in Table(3) for each pellet.

Table 3: The physical characteristics of the $(Zn_{(1-x)}Al_x)$O pellets, for $x = 0.005, 0.01, 0.015, 0.02, 0.025, and\ 0.03$ at $300K$.

$(Zn_{(1-x)}Al_x)O$	x	$S(\mu V/K$	$\sigma\ (s/m)$	$R_H(cm^3C^{-1})$	$n \times (cm)^{-3}$
$ZnO_{0.995}Al_{0.005}$	0.005	-4.60067	305.9658	8.48233	-7.36826E+17
$ZnO_{0.99}Al_{0.01}$	0.01	-2.43289	890.2125	4.94741	-1.26329E+18
$ZnO_{0.985}Al_{0.015}$	0.015	-3.69128	929.6679	2.4402	-2.56126E+18
$ZnO_{0.98}Al_{0.02}$	0.02	-4.87584	177.0284077	2.42268	-2.5798E+18
$ZnO_{0.975}Al_{0.025}$	0.025	-3.77248	2151.388	1.16005	-5.38771E+18
$ZnO_{0.97}Al_{0.03}$	0.03	-3.80872	1637.178	3.97992	-1.57038E+18

Figure 7 displays the power factor ($PF = S^2\sigma$) the letters PF and S stand for power factor and absolute Seebeck coefficient, respectively, while σ stands for electrical conductivity [12], of the sintered samples as a function of temperature. The PF is dependent upon S and σ. [32]. A higher PF is going to be the result of increases in both S and σ. The PF changes as the temperature changes, The performance of a thermoelectric material was measured by its PF, hence this value is the efficiency of a thermoelectric material and thus serves as a sign for thermoelectric materials. A thermoelectric material's PF is the component responsible for regulating its comprehensive electrical characteristics. The higher PF $(Zn_{(1-x)}Al_x)O$ with $x = 0.02$, $\sim 1300(\frac{\mu w}{mk^2})$ at $580K$, this resulted from the comparatively high S content of the sample and had the highest PF values when compared to other samples described in earlier studies [33-35].

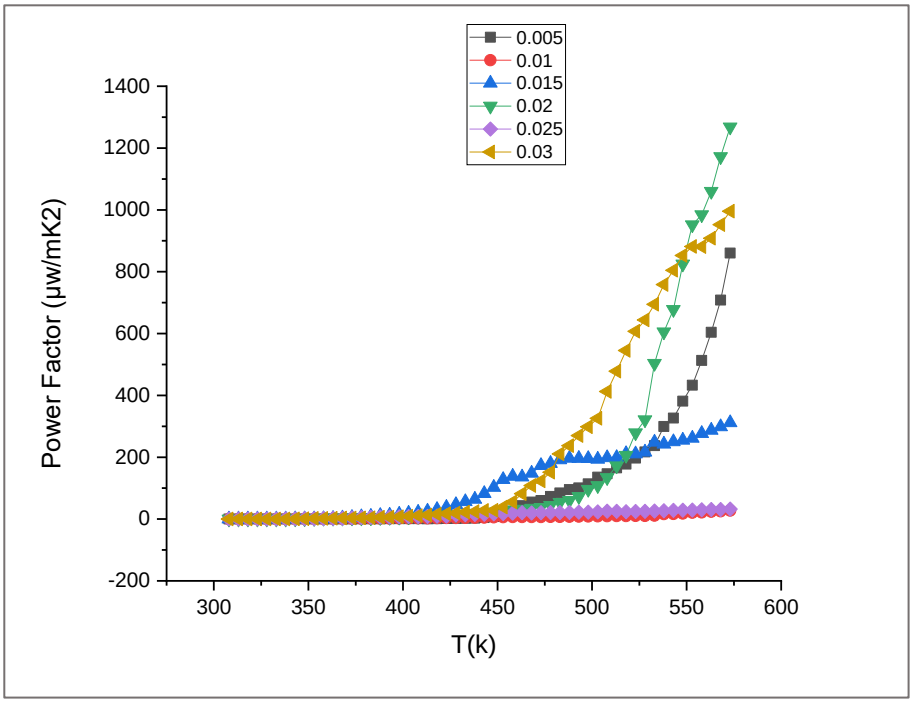

Figure 7: The power factor of the $(Zn_{(1-x)}Al_x)O$. pellet with $x = 0.005, 0.01, 0.015, 0.02, 0.025, and\ 0.03$.

4. Conclusion

The n-type $(Zn_{(1-x)}Al_x)O$ with $x = 0.005 - 0.03$ was synthesized using a solid-state technique, which is a quicker, simpler, and more cost-effective interfacial reaction. The study examined the samples' structural, morphological, electrical, and thermoelectrical properties. It was determined via analysis of structural characteristics that all samples are hexagonal structures. The present study shows that the Seebeck coefficient was negative for all samples of $(Zn_{(1-x)}Al_x)O$, and it also demonstrated an enhanced power factor This method of synthesis, in conjunction with the donor dopant activity of Al^{3+} in ZnO, has not only led to an increase in carrier concentration (and thus an increase in electrical conductivity), but it has led to a decrease in grain growth, and this is of much more significance. Finally, we can conclude that the process of sintering a thermoelectric material at a temperature of $1273\ K$ plays a significant role in improving the thermoelectric properties of the material.

Reference

1. Zheng, X., et al., A review of thermoelectrics research–Recent developments and potentials for sustainable and renewable energy applications. Renewable and Sustainable Energy Reviews, 2014. **32**: p. 486-503.
2. Ohtaki, M., K. Araki, and K. Yamamoto,High thermoelectric performance of dually doped ZnO ceramics. Journal of Electronic Materials, 2009. **38**: p. 1234-1238.
3. Zaitsev, V., et al., Thermoelectrics handbook: macro to nano. Ed. DM Rowe, CRCpress Taylor & Francis, Boca Raton, 2006: p. 29-1.
4. Bell, L.E., Cooling, heating, generating power, and recovering waste heat with thermoelectric systems. Science, 2008. **321**(5895): p. 1457-1461.
5. Safeer, S.H., et al., Suppression of Superconductivity by Anharmonic Oscillations in Zn-or Ni-doped Cu 0.5 Tl 0.5 Ba 2 (CaMg) Cu 1.5 M 1.5 O 10-δ (M= Zn, Ni) Superconductors; Evident by Magnetic Measurements. Journal of Electronic Materials, 2021. **50**: p. 6518-6524.
6. Latronico, G., et al., Synthesis and characterization of Al-and SnO2-doped ZnO thermoelectric thin films. Materials, 2021. **14**(22): p. 6929.
7. Backhaus-Ricoult, M., et al., Semiconducting large bandgap oxides as potential thermoelectric materials for high-temperature power generation? Applied Physics A, 2014. **116**(2): p. 433-470.
8. Lin, B., Z. Fu, and Y. Jia, Green luminescent center in undoped zinc oxide films deposited on silicon substrates. Applied physics letters, 2001. **79**(7): p. 943-945.
9. Mohammed, M., et al., A review of thermoelectric ZnO nanostructured ceramics for energy recovery. International Journal of Engineering & Technology, 2018. **7**(2.29): p. 27-30.
10. Park, K., et al., Enhanced high-temperature thermoelectric properties of Ce-and Dy-doped ZnO for power generation. Energy, 2013. **54**: p. 139-145.
11. Janotti, A. and C.G. Van de Walle, New insights into the role of native point defects in ZnO. Journal of Crystal Growth, 2006. **287**(1): p. 58-65.
12. Ullah, M., et al., Thermoelectric properties, phase analysis, microstructural investigation and lattice parameters c/a ratio of Al3+ and In3+ dual-doped zinc oxide-based ceramics sintered at high temperature under an argon atmosphere. Materials Science in Semiconductor Processing, 2018. **87**: p. 202-206.
13. Yang, S., et al., Enhanced power factor of textured Al-doped-ZnO ceramics by field-assisted deforming. Journal of the American Ceramic Society, 2017. **100**(4): p. 1300-1305.
14. Zakharchuk, K.V., et al., A self-forming nanocomposite concept for ZnO-based thermoelectrics. Journal of Materials Chemistry A, 2018. **6**(27): p. 13386-13396.
15. Ohtaki, M., et al., High-temperature thermoelectric properties of (Zn1− x Al x) O. Journal of applied physics, 1996. **79**(3): p. 1816-1818.
16. Tsubota, T., et al., Thermoelectric properties of Al-doped ZnO as a promising oxide material for high-temperature thermoelectric conversion. Journal of Materials Chemistry, 1997. **7**(1): p. 85-90.
17. Sajjad, M., et al., Structural and optical properties of pure and copper doped zinc oxide nanoparticles. Results in Physics, 2018. **9**: p. 1301-1309.
18. Isram, M., et al., Thermoelectric and Structural Properties of Sputtered AZO Thin Films with Varying Al Doping Ratios. Coatings, 2023. **13**(4): p. 691.
19. Monshi, A., M. Foroughi, and M. Monshi, Modified Scherrer equation to estimate more accurately nano-crystallite size using XRD. World J Nano Sci Eng 2 (3): 154–160. 2012.
20. Monshi, A., M.R. Foroughi, and M.R. Monshi, Modified Scherrer equation to estimate more accurately nano-

crystallite size using XRD. World journal of nano science and engineering, 2012. **2**(3): p. 154-160.
21. Giovannelli, F., et al., Thermal conductivity and stability of Al-doped ZnO nanostructured ceramics. Journal of the European Ceramic Society, 2018. **38**(15): p. 5015-5020.
22. Jantrasee, S., P. Moontragoon, and S. Pinitsoontorn, Thermoelectric properties of Al-doped ZnO: experiment and simulation. Journal of Semiconductors, 2016. **37**(9): p. 092002.
23. Mayandi, J., et al., Al-doped ZnO prepared by co-precipitation method and its thermoelectric characteristics. Materials Letters, 2021. **288**: p. 129352.
24. Radingoana, P.M., et al., Microstructure and thermoelectric properties of Al-doped ZnO ceramic prepared by spark plasma sintering. Journal of the European Ceramic Society, 2023. **43**(3): p. 1009-1016.
25. Hong, M.-H., et al., Thermoelectric properties of Al-doped mesoporous ZnO thin films. Journal of Nanomaterials, 2013. **2013**: p. 1-1.
26. Ullah, M., et al., Thermoelectric properties of Al-doped zinc oxide-based ceramics sintered at high temperature under different atmospheres. Journal of Materials Science: Materials in Electronics, 2019. **30**: p. 8611-8618.
27. Li, D., R. Sun, and X. Qin, Thermoelectric properties of p-type (Bi2Te3) x (Sb2Te3) 1− x prepared by spark plasma sintering. Intermetallics, 2011. **19**(12): p. 2002-2005.
28. Hmood, A., A. Kadhim, and A.H. Haslan. Fabrication and characterization of pb1-xYbxSe0. 2Te0. 8 based alloy thin films thermoelectric generators grown using thermal evaporation method. in Materials Science Forum. 2013. Trans Tech Publ.
29. Abd Alkadhim, A.H., The Effects of Ytterbium Doping Upon the Structural and Electrical Transport Properties of Lead Chalcogenide Alloy Thin Films for Thermoelectric Applications. 2013, Universiti Sains Malaysia.
30. Kadhim, A., A. Hmood, and H. Abu Hassan, Effect of Se Substitution on Structural and Electrical Transport Properties of Bi 0.4 Sb 1.6 Se 3 x Te 3 (1− x) Hexagonal Rods. Journal of electronic materials, 2013. **42**: p. 1017-1023.
31. Ghazi, N. and A. Kadhim, Thermoelectric properties of solid state reaction-prepared ZnO based alloys with various CuO doping in (CuO) x (ZnO) 1− x. Solid State Communications, 2023. **361**: p. 115058.
32. Tian, T., et al., Defect engineering for a markedly increased electrical conductivity and power factor in doped ZnO ceramic. Acta Materialia, 2016. **119**: p. 136-144.
33. Virtudazo, R.V.R., et al., Improvement in the thermoelectric properties of porous networked Al-doped ZnO nanostructured materials synthesized via an alternative interfacial reaction and low-pressure SPS processing. Inorganic Chemistry Frontiers, 2020. **7**(21): p. 4118-4132.
34. Constantinescu, G., et al., Enhancement of Thermoelectric Performance of Donor-Doped ZnO Ceramics by Involving an In Situ Aluminothermic Reaction during Processing. Crystals, 2022. **12**(11): p. 1562.
35. Zhou, B., et al., Significant enhancement in the thermoelectric performance of aluminum-doped ZnO tuned by pore structure. ACS Applied Materials & Interfaces, 2020. **12**(46): p. 51669-51678.

1.